ACS NANO

www.acsnano.org

ARTICLE

Weavable, Reconfigurable Triboelectric Ferrofluid Fiber for Early Warning

Naiyan Wu,[7] Pengxiang Mao,[7] Ningbo Chang,[7] Yanrun Zhou, Weifeng Yang, Fan Fu, Xixi Liu, Tianyi Ji, Junyi Zhao, Yuxuan Huang, Yaogang Li,* Michael D. Dickey, and Wei Gong*

Cite This: *ACS Nano* 2024, 18, 33319−33329

Read Online

ACCESS | Metrics & More | Article Recommendations | Supporting Information

ABSTRACT: **As communication technologies have become omnipresent, the prevalence of electromagnetic field (EMF) exposures poses possible health risks, particularly to vulnerable groups such as pregnant women. In response, we introduce a triboelectric ferrofluid fiber (TFF) that moves in response to EMF, thereby generating charge in a way that is self-powered. The TFF is flexible, stretchable (470%), and can be woven into fabrics. The TFF utilizes a soft-contact (ferrofluid-silicon rubber fiber) triboelectric core layer to enhance its sensitivity to EMF, enabling it to detect even minor electromagnetic fluctuations, such as those from cell phone typing. By integrating hydrogel electrodes that offer conductivity and minimal electromagnetic interference shielding, the TFF's sensitivity to magnetic fields is further amplified. Moreover, its open-circuit voltage output is increased by 50% compared to the conventional electrodes. Building on this technology, we designed a smart fabric for environmental early warning and potential real-time pulse monitoring, specifically tailored for the safety and healthcare needs of vulnerable groups. Finally, we developed a sensing and communication apparel (SCA) by integrating TFF into the apparel and exploring its capabilities in a wireless transmission of warning signals and long-distance NFC functionality.**

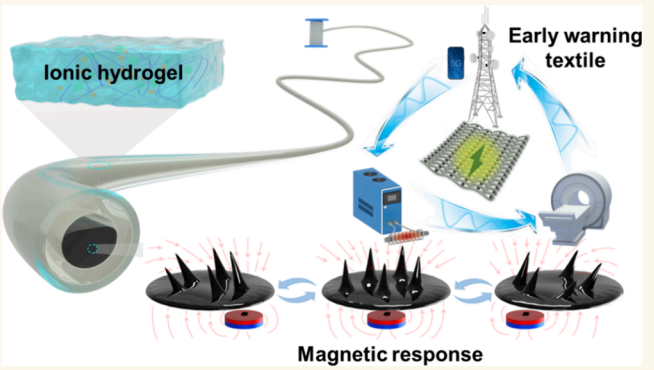

KEYWORDS: *ferrofluid fiber, triboelectric soft contact, magnetically responsive textiles, environment early warning, large-scale production*

INTRODUCTION

Annually, there are over 200 million pregnancies, a critical stage in life characterized by profound physiological and behavioral transformations.[1,2] The environments and lifestyles of pregnant individuals are crucial, impacting both their own health and the development of the fetus.[3] Recent research underscore the significant risks posed by high levels of magnetic fields and intense electromagnetic radiation, which can disrupt the chemical stability of cellular tissues, triggering apoptosis and stunting embryonic growth. These disruptions increase the probability of health risks in pregnant women and fetal malformations.[4−6] These findings emphasize the necessity of developing a portable automatic early warning sensing system that can alert in the presence of dangerous magnetic and electromagnetic environments to safeguard the health of vulnerable groups, especially pregnant women.[3,7−9]

Conventional EMF sensors are typically bulky, and rigid, and often require complex supplementary circuitry, making them unsuitable for portable wearable devices.[10,11] Recent advancements in flexible materials and wearable sensing are increasingly prominent due to technological innovations.[12−22] However, the frequent need for maintenance and replacement of traditional power systems, and the low integration with clothing continue to slow the development of wearable EMF sensing technology. Self-powered sensing fibers are characterized by their high weavability and independence from external power sources, making them a promising candidate for the next generation of wearable EMF sensors.[23−26] Despite its promise, the self-powered sensing fibers' application is currently limited by its poor abrasion resistance and suboptimal electrical output.[27] A significant issue is that conventional solid electrode materials tend to have a strong electromagnetic interference shielding effect (EMI SE),[28,29] considerably reducing their sensitivity to electromagnetic

Received: May 11, 2024
Revised: November 14, 2024
Accepted: November 22, 2024
Published: November 29, 2024

https://doi.org/10.1021/acsnano.4c06225
ACS Nano 2024, 18, 33319−33329

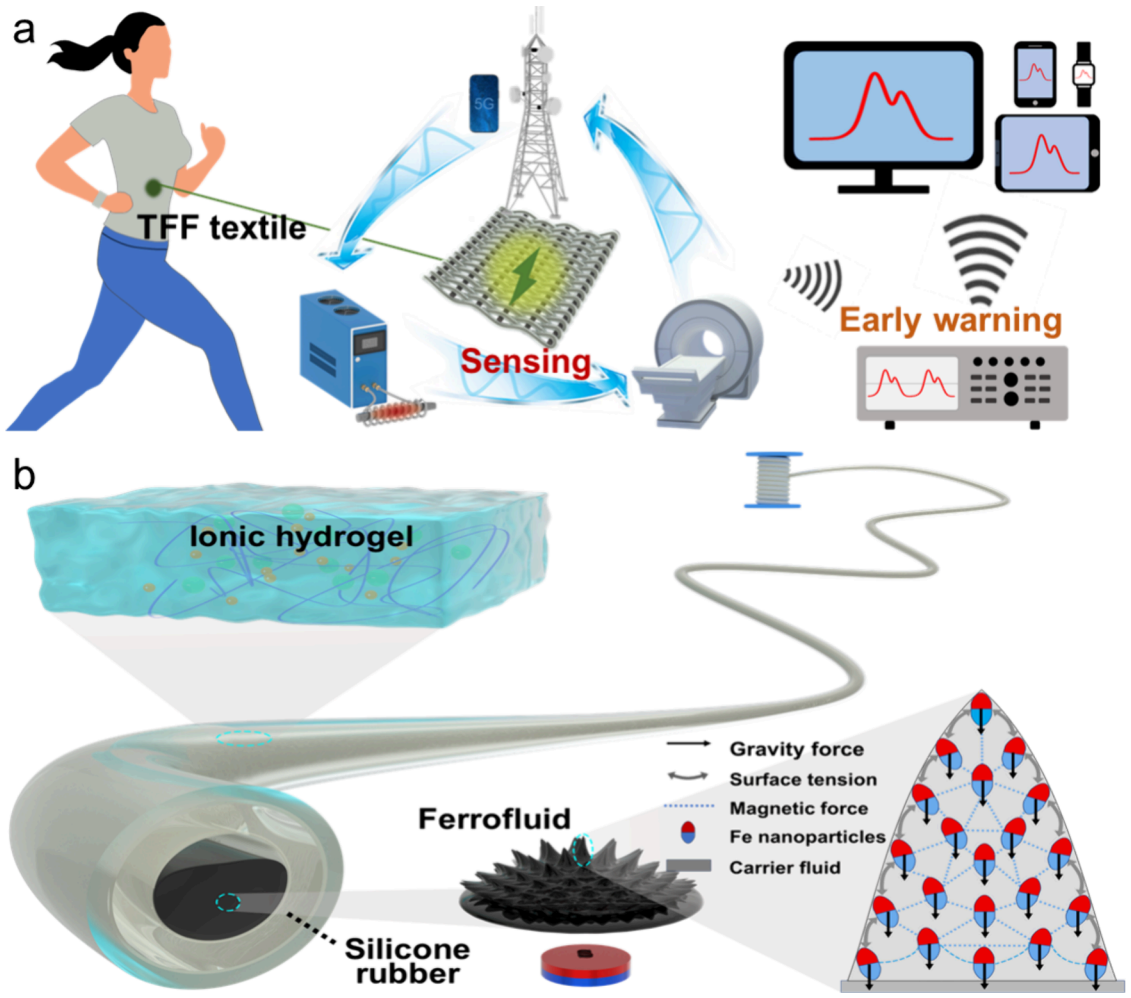

Figure 1. (a) Schematic illustration of self-powered smart sensing platform. (b) Schematic illustration of the TFF.

waves and magnetic fields.[30,31] Furthermore, the performance of traditional designs is significantly influenced by environments,[32,33] posing a considerable challenge to their practical use in smart wearable sensors.

Here, we present magnetically responsive, self-powered triboelectric ferrofluid fiber (TFF) designed for EMF sensing. The TTF consists of a hollow silicone fiber filled with ferrofluid internally and coated with hydrogel externally. This combination of materials results in a highly flexible and stretchable fiber (up to 470%) that can be woven into a textile. The fabrication process is compatible and designed for large-scale production. The fibers generate tribocharge in response to EMFs due to the moving of the ferrofluid and its interaction with the silicone walls. The internal magnetic response of the TFF core enables it to maintain its sensing performance unaffected by humidity, utilizing the capability of magnetic fields to penetrate water with minimal strength loss. Additionally, the ion-conducting hydrogel electrode sheath enhances the response of TFF to magnetic fields and boosts the open-circuit voltage output by 50% compared to the conventional electrodes. We demonstrate a self-powered textile with an environment early warning platform and explore the potential for real-time pulse monitoring. Finally, we successfully integrated TFF into apparel to create an electronic textile (e-textile), the Sensing and Communication Apparel (SCA). By incorporating a mobile terminal, Bluetooth module, and induction coils, the SCA can wirelessly transmit open-circuit voltage signals generated by magnetic fields to the mobile terminal and offer long-distance NFC functionality.

RESULTS AND DISCUSSION

The self-powered environment early warning smart textile platform, shown in Figure 1a, is woven from TFFs capable of sensing changes in EMFs and constant magnetic fields in the environment. To maintain the attractive features of stretchable fibers, each constituent element in the TTF is engineered using materials with flexibility and stretchability.[34,35] The composition of TFF is shown in Figure 1b, incorporating water-based ferrofluids (tribo-positive material), hollow silicone rubber fibers (tribo-negative material), and a coating of ionically conductive hydrogel, which serves as an external electrode.

Ionic hydrogel electrodes coated on the exterior of TFFs are important for the performance of the fibers. Hydrogels are attractive as electrodes for several reasons. First, they are soft and stretchable. Second, they do not shield EMF in a pronounced way like conventional metals. Third, they are biocompatible.[36−38] In this work, a hydrogel electrode sheath was coated coaxially around the silicone rubber fibers to enhance the electrical output performance of the TFF compared to conventional electrodes and the ionic hydrogel shows excellent biocompatibility (Figure S1). A soft-molding method (refer to synthesis of TFF) was designed to pass the

https://doi.org/10.1021/acsnano.4c06225
ACS Nano 2024, 18, 33319−33329

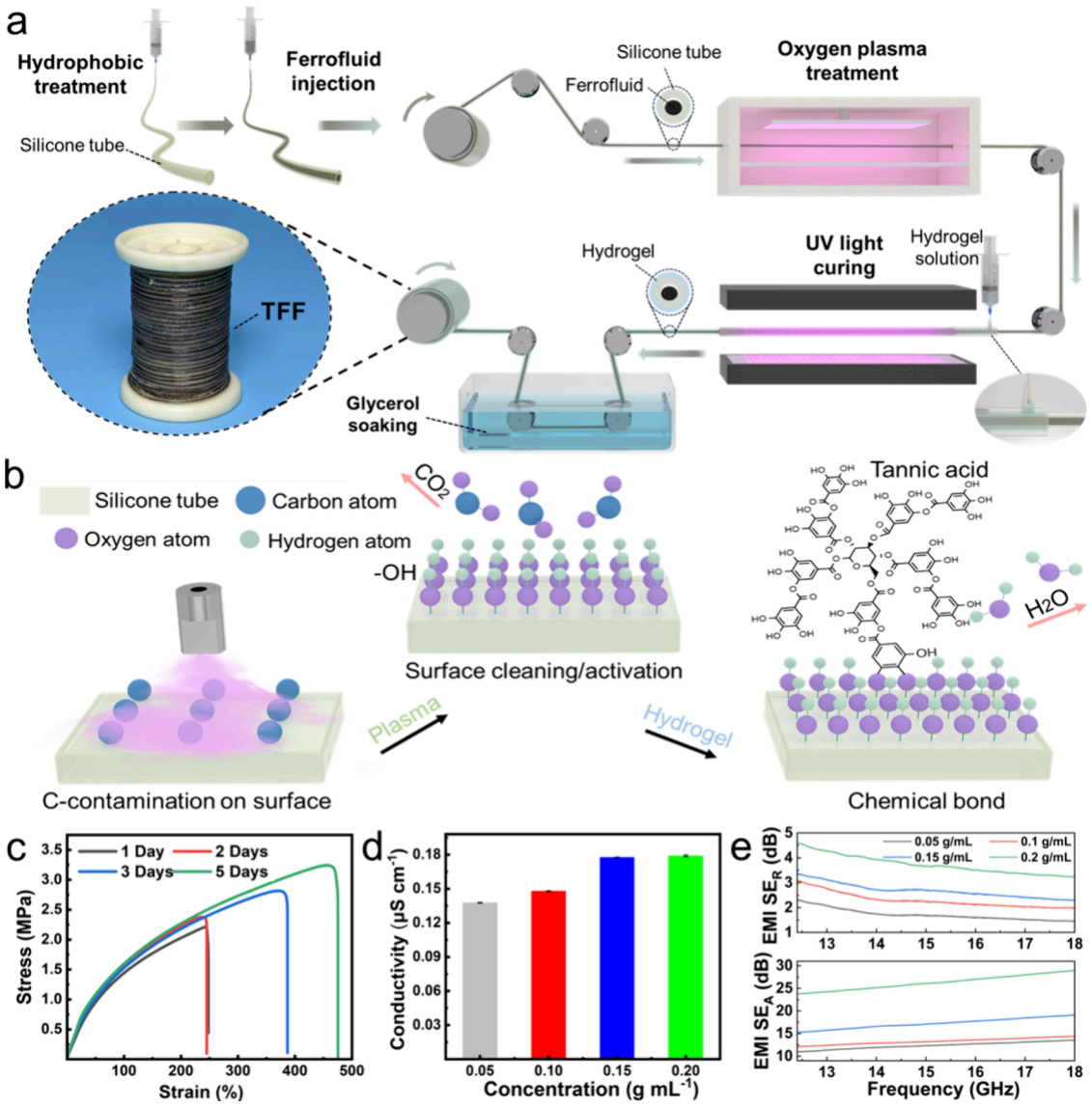

Figure 2. (a) Schematic diagram of the preparation process of TFF and TFF collected with collection roller. (b) Schematic diagram of the bonding of the adhesion factor tannic acid on the surface of silicone rubber after oxygen plasma treatment. (c) The effect of aging time on the stretchability of the TFF. (d) Conductivity of hydrogel electrodes with different NaCl concentrations. (e) The SE_R and SE_A at different frequencies for hydrogel electrodes with different ionic concentrations.

fibers through a plasma and a UV curing chamber. The plasma improves the adhesion to the gel[39] and the UV chamber cures the gel coating. The fibers are collected on a roller to achieve large-scale preparation of TFF (Figure 2a). Tannic acid was included in the gel to promote adhesion via the large number of −OH groups, which react with the −OH groups on the surface of the silicone rubber fibers in a dehydration reaction (Figure 2b) to produce chemical adhesion, which tightly binds the hydrogel electrode sheaths to the silicone rubber interface.[40,41] The tannic acid molecules also form a large number of reversible chemical bonds (hydrogen bonds) with the polyacrylamide chains giving the hydrogel electrodes excellent self-healing capabilities (Figure S2). In addition, the axial contraction of the gel during curing allows it to bond more tightly to the silicone rubber (Figure S3). Under the strong binding force, the standard-size (0.8 × 2 cm) hydrogel electrode combined with silicone rubber can withstand a 50 g weight without falling off (Figure S4). N, *N*′-methylenebis (acrylamide), acting as a cross-linking agent, reacts with acrylamide to form a cross-linked network that confers strength to the hydrogel electrode.[42,43] To avoid the attenuation of TFF properties due to dehydration, we soaked the prepared triboelectric ferrofluid fiber in a 70% glycerol solution for 30 min. This process improved the water retention properties of the hydrogel electrodes without compromising their other characteristics (Figure S5). After 2 days at room temperature, the mechanical properties will be enhanced due to the topological reorganization practiced by the ionic hydrogel, and the tensile strength can reach 800%.[44] The properties do not change much after 5 days (Figure S6). Figure S7 illustrates various deformations of TFF, including stretching, bending, twisting, and winding, which do not affect the electrical output performance of the TFF (Figure S8). Due to its good sealing, the TFF is also less susceptible to environmental changes such as temperature and humidity (Figure S9). Further analysis shows that the adhesion between the hydrogel and the silicone rubber tubing was enhanced by axial shrinkage caused by dehydration, as shown in Figure 2c, and thus the TFF could

https://doi.org/10.1021/acsnano.4c06225
ACS Nano 2024, 18, 33319−33329

maintain its optimal tensile properties after 5 days with a tensile of 470%. The tight bonding between the hydrogel electrode sheath and the friction core layer contributes to TFFs' excellent abrasion resistance, which is further enhanced when combined with fabric (Figure S10). Additionally, the conductivity and total EMI SE (EMI SE_T) of hydrogel electrodes were evaluated across various sodium chloride (NaCl) concentrations in the gel. The conductivity of hydrogel electrodes with ionic concentrations of 0.15 g/mL and 0.2 g/mL were close (Figures 2d). The total EMI SE_T is the contributions of shielding reflection (SE_R) and shielding absorption (SE_A). As shown in Figure 2e, when the concentration increases from 0.15 g/mL to 0.2 g/mL, the SE_A value shows a substantial rise, leading to a steep increase in the absorption of electromagnetic waves. This results in a significant increase in EMI SE_T (Figure S11a), which in turn causes the attenuation of the TFF's electrical output. The imaginary part (ε_M) of the microwave dielectric constant is also compatible with the EMI SE_T results (Figure S11b). Thus, the best combination of high conductivity and low EMI SE of hydrogel electrode was hypothesized to occur at a NaCl concentration of 0.15 g/mL, a proposition we intended to validate in subsequent tests.

The development of the hydrogel coating offers insights into augmenting the electrical output performance of TFF by mitigating interference. Here, we aim to further enhance TFF's electrical output through the design and modification of the triboelectrification materials involved. Ferrofluid is a colloidal suspension that includes a blend of nanoparticles with permanent magnetic dipoles and surface charges, a carrier fluid, and a surfactant.[45−48] The interactions between the particles, including van der Waals forces, screened electrostatic repulsions, and magnetic dipolar interactions, cause the ferrofluid to lay flat in the silicone rubber fibers surface and exhibit fluid mobility when there is no magnetic field.[49,50] When exposed to a magnetic field, the particles in the ferrofluid align into a conic array through the Rosensweig instability. As illustrated in Figure 3a, upon application of a direction-variable magnetic field, the orientation of the conic array assembly shifts to the direction opposite to that of the magnetic field. The corresponding optical and magnified images can be observed in Figures 3b and 3c. During the rotational movements of the magnet, the shape of the macro array remains stable, ensuring the stability of TFF after long-term use (Figure S12), which benefits from the uniform dispersion of ferromagnetic nanoparticles in the carrier fluid. The SEM images of the magnetic nanoparticles are shown in Figures 3d and 3e. In the presence of an external magnetic field, these nanoparticles arrange themselves into chains or columns. When the magnetic field is removed, the microstructure disintegrates, and the magnetism dissipates (Figure S13). This paramagnetic behavior allows the magnetic fluid to respond dynamically to the magnetic field, enhancing its ability to facilitate electrical contact and separation through friction.

Then, a double helix extruder with a surface-texture spinneret die was used to prepare silicone rubber fibers with complex microstructures in the inner wall (Figure S14), which increases the surface area and thus the contact charging area between the triboelectric layers, ultimately boosting TFF sensitivity compared to other works (Figure S15 and Table S1). However, these minor depressions facilitate the adherence with the magnetic fluid during motion, leading to a diminished electrical output performance of TFF. Impregnation with 1H,

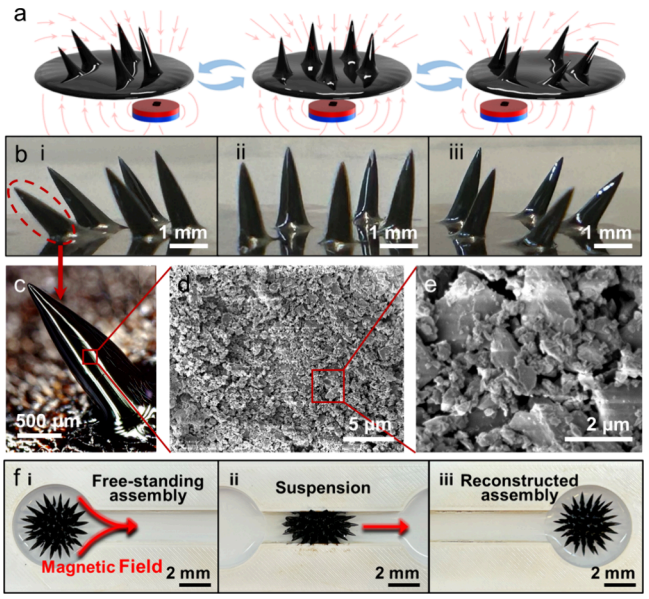

Figure 3. (a) Schematic diagram of the dynamic movement of the conic arrays under a direction-variable magnetic field. (b) Photographs of left-tilt, vertical and right-tilt of conic arrays of ferrofluid. (c) Magnified photograph of an individual magnetic fluid spike. (d and e) SEM images of magnetic nanoparticles in ferrofluid under different magnifications. (f) Manifestation for the assembly and reconstruction process of ferrofluid on hydrophobically treated silicone rubber substrate.

1H, 2H, 2H-perfluorodecyltriethoxysilane (PFDTES) was used to modify the chemistry of the silicone walls to render it hydrophobic[51] (Figure S16). The enhanced hydrophobicity[52] leads to an increase in the water contact angle from 71° to 145.7° (Figure S17). The reduced resistance to liquid flow can contribute to the response time of TFFs (Figure S18). Figure 3f illustrates the assembly and reconstruction of ferrofluid on a hydrophobic silicone rubber substrate. Initially, an independent conic array is preformed on the left panel under a magnetic field, as seen in (Figure 3f i). By manipulating the magnetic field, this conical array rapidly changes shape and passes from left to right through a narrow channel (Figure 3f ii). Subsequently, a reformed conic array is established on the right panel (Figure 3f iii). Throughout the entire process, the magnetic fluid remains nonadhesive to the silicone rubber substrate. Ferrofluid and silicone rubber fibers with hydrophobic treatment form the triboelectric core layer. To overcome the adverse effects of fluid resistance and increase the ferrofluid injection rate into silicone rubber fibers, we also optimized the process using a dual-force injection method. Combined with the hydrophobic treatment, we have achieved continuous, stable, efficient and long-distance injection of ferrofluids into silicone rubber tubing (Figure S19).

Figure S20 simulates the morphological changes of the ferrofluid and triboelectric charges within the silicone rubber fiber. In the absence of a magnetic field, the ferrofluid stays stationary. When a weak magnetic field is applied, small conical spikes begin to form on the surface, which lengthens as the magnetic induction increases or the distance between the TFF and the magnetic field decreases (Figure S21). Induced charges are generated where the ferrofluid contacts the inner wall of the fiber as the ferrofluid starts to congregate toward the center of the magnetic field. Once the ferrofluid is completely centralized, the relative change of the contact area between the

https://doi.org/10.1021/acsnano.4c06225
ACS Nano 2024, 18, 33319−33329

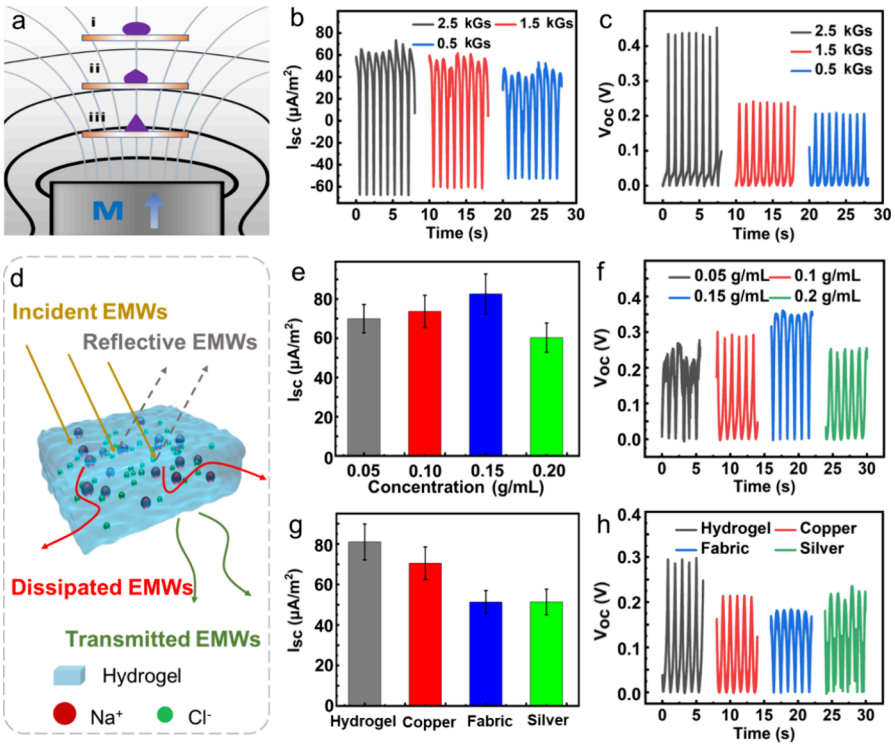

Figure 4. (a) Shape changes of ferrofluid droplets with magnetic field intensity. (b and c) Short-circuit current (b) and open-circuit voltage (c) performance of TFF in different magnetic intensities. (d) Schematic illustration of refraction and dissipation of electromagnetic waves by hydrogel electrodes. (e and f) Short-circuit current (e) and open-circuit voltage (f) performance of TFF prepared with different NaCl concentrations. (g and h) Short-circuit current (g) and open-circuit voltage (h) performance of TFF prepared by hydrogel electrodes with different electrode materials.

ferrofluid and the silicone rubber fiber is at its largest, and the amount of induced charge generated reaches a maximum. This mechanism allows the TFF to maintain consistent electrical output performance under arbitrary deformation even when the internal ferrofluid is not continuous (Figure S22). Figure S23 simulates the contact phenomenon between the ferrofluid and the silicone rubber fiber by constructing an electron cloud interaction model. Before contact, electrons occupy their respective atomic orbitals and are loosely bound in a potential well, forming an electron cloud. Upon contact between the two materials, the electron clouds overlap, and the original single potential well evolves into a double asymmetric potential well, powering the transfer of electrons. When the external conditions (e.g., temperature) are constant, once the two materials are separated, the transferred electrons remain in the orbitals due to the existence of energy barriers within the materials, creating a potential difference at the friction interface. The operational principle of the TFF is also confirmed in COMSOL finite element simulations, as depicted in Figure S24.

The ferrofluid droplet changes shape from ellipsoidal to conical when it moves closer to the magnetic field, as depicted in Figure 4a. As the distance between the two objects gets smaller, the cone's height rises, improving the TFF's electrical output performance. The capacity to generate highly sensitive electrical signals at varying magnetic induction strengths highlights its potential for use in wearable sensor devices (Figures 4b, 4c, and S25). A 10 cm length TFF was fixed on one side of the linear motor, and magnets were applied with different magnetic inductions on the opposite side to control reciprocating motion (Figure S26). We precisely regulated the magnetic field strength around the TFF by using different strengths of rubidium permanent magnets and adjusting the distance between the magnets and TFF (Figure S27). The results indicate that the short-circuit current increased from 50 $\mu A/m^2$ to 70 $\mu A/m^2$ (current normalized by the inner surface area of the fiber) and the open-circuit voltage escalated from 0.2 to 0.45 V with the increase in magnetic flux density. The magnetic force exerted by the magnet on the ferrofluid is proportional to the magnetic induction strength, and as the magnetic force increases, the ferrofluid makes more thorough contact with the silicone rubber fiber wall. This process improves the effective contact area, subsequently enhancing the electrical output. The ionic concentration of the hydrogel electrode is also a crucial factor affecting the electrical output of TFF. Electromagnetic waves (EMW) dissipate after many internal refractions between the salt ions of the hydrogel (Figure 4d). By modulating the NaCl concentration within the hydrogel electrode, one can regulate the transmittance of EMWs, thereby achieving precise control over EMI SE. To identify the optimal formulation that offers both superior conductivity and electromagnetic shielding capabilities, we investigated the impact of varying NaCl concentrations in hydrogel electrodes on the electrical output characteristics of TFF (Figures 4e, 4f and S28). The outcome indicates that the electrical performance of TFF initially rises as the NaCl concentration increases. The short-circuit current density (80 $\mu A/m^2$) and open-circuit voltage (0.35 V) of the TFF reached maximum when the sodium chloride concentration was 0.15 g/mL. With a further increase in concentration, the electrical performance was constrained by the electromagnetic shielding effectiveness, resulting in a decrease in the electrical output.

https://doi.org/10.1021/acsnano.4c06225
ACS Nano 2024, 18, 33319−33329

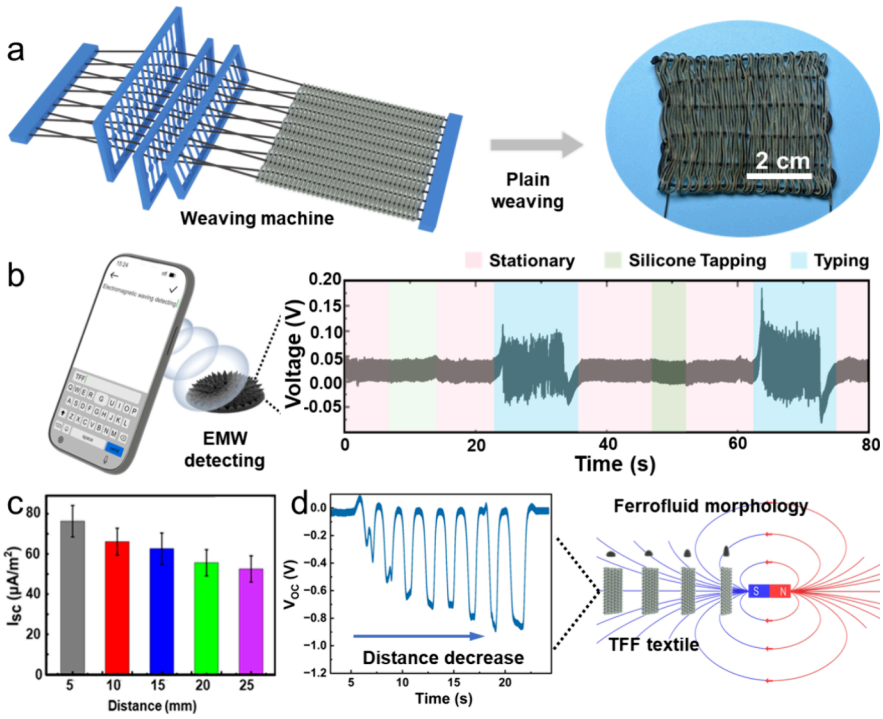

Figure 5. (a) Fabrication of TFF textile by plain weaving. (b) The open-circuit voltage output of the TFF e-textile in three scenarios: at rest, tapping with a rubber mallet, and typing with a hand. (c) Short-circuit current performance at different distances between the TFF and the magnetic field. (d) Open-circuit voltage signal generated when TFF textile approaching magnetic field.

Figures 4g, 4h and S29 compare the electrical output performance of TFF prepared with different electrode materials (Figure S30). The results showed that TFF with ionic hydrogel electrodes had the best performance with a short-circuit current density of 80 $\mu A/m^2$ and an open-circuit voltage of 0.30 V, which is a 50% improvement compared to copper and silver electrodes. The incorporation of hydrogel electrodes in TFF significantly boosts its electrical output by avoiding the electromagnetic shielding effect of conventional solid electrode materials while maintaining excellent electrical conductivity. Additionally, owing to the inherent liquid nature of the ferrofluid, which resonates when subjected to external vibrations, we also measured the voltage signals generated by TFF under various impact forces (Figure S31).

Strong electromagnetic radiation has negative impacts on human health, potentially leading to fatigue, headaches, reduced learning ability, and cognitive impairment.[53−55] The effects are even more serious in vulnerable groups such as pregnant women, where prolonged radiation exposure increases the risk of health complications and irreversible effects on immune function, and even raises the possibility of fetal malformations.[6,56−58] Here, we developed a self-powered smart textile using plain weaving to integrate TFF into the textile, providing environmental alerts and a real-time health monitoring system for vulnerable groups (Figure 5a). TFF is ultrasensitive to electromagnetic waves and can detect electromagnetic waves generated by the tiny currents of cell phone typing.[59] We placed TFF close to a cell phone and connected it to the electrometer, electromagnetic waves produced by cell phone usage can be successfully detected and converted into an electrical signal output, as depicted in Figure 5b. TFF produces a stable electrical output when the phone is inactive, but while typing, changes in the electromagnetic waves emitted by the phone cause a constant fluctuation in the electrical output, which later stabilizes again once typing stops (Figures S32a, S32b and Video 1). We excluded the possibility that the electrical output signal is generated by human artifacts through control experiments (Figure S32c and Video 2). By artificially setting a human safety threshold value (4 kGs),[60] the TFF can sense changes in the surrounding electromagnetic waves and trigger an alarm when the generated electrical output signal exceeds the threshold, thus acting as an early warning system for strong electromagnetic waves. Additionally, the TFF is also sensitive to stationary magnetic fields, generating electrical output in their proximity. This is evident in Figures 5c and S33, where the electrical signal output increases as the TFF gets closer to the magnetic field, with the short-circuit current increasing from 50 $\mu A/m^2$ to 75 $\mu A/m^2$ and the open-circuit voltage rising from 0.15 to 0.3 V. As shown in Figure 5d, we placed the TFF textile close to a fixed magnetic field, and the resulting open-circuit voltage signal varies in magnitude depending on the distance. When the safety threshold is set to 4 kGs, the TFF textile will alert if the safe distance between user and stationary magnetic field is not maintained. In practical applications, short pauses can be used to avoid interference from motion artifacts, ensuring accurate TFF measurements during continuous motion. With an ultrafast response time of 0.13 s, the TFF provides reliable readings even during brief pauses, clearly distinguishing stable signals at rest from the irregular signals generated during movement. This approach effectively minimizes the impact of motion disturbances, ensuring consistent measurement accuracy in practical settings (Figure S34). Finally, since TFF is capable of sensing mechanical forces, we also explored the potential of TFF as a real-time pulse detection system. As shown in Figure S35, each signal wave represents a pulse beat and the density of the signal wave indicates the pulse frequency. TFF generates an

https://doi.org/10.1021/acsnano.4c06225
ACS Nano 2024, 18, 33319−33329

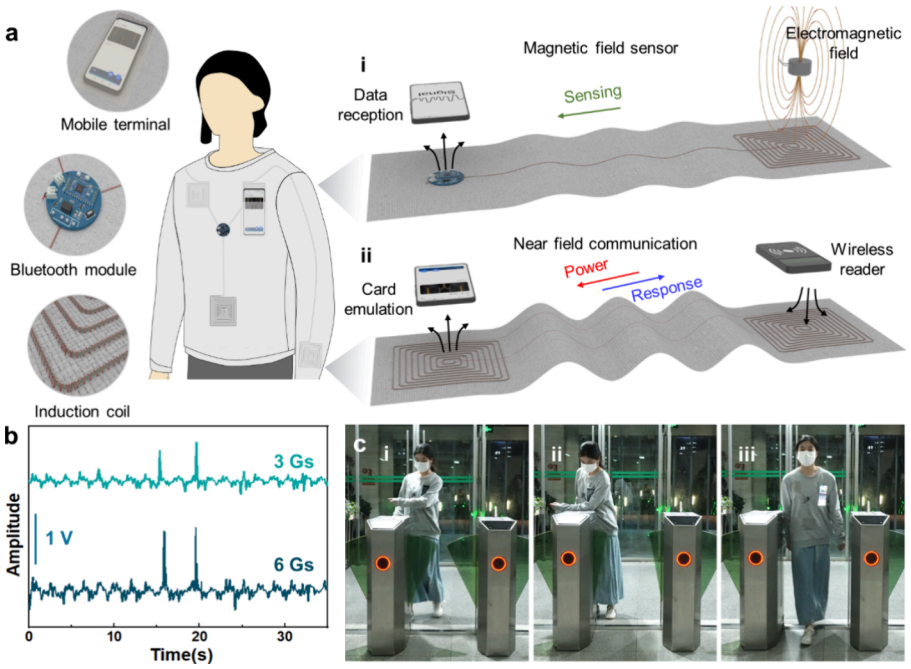

Figure 6. (a) Schematic illustration of magnetic field sensing via Bluetooth (i) and NFC functionality (ii) of SCA. (b) The open-circuit signals of SCA sensing to magnetic fields with different strengths via Bluetooth. (c) Photograph of a free physical card passing through the gate using SCA's NFC function.

electronic output signal that varies with the frequency and intensity of the pulse, enabling real-time pulse monitoring.

Finally, we used TFF to develop a SCA that can sense external magnetic environments. We first enhanced the mechanical properties and reduced the diameter of TFFs through mechanical training, thereby improving their textile properties (Figure S36). Then, using computer-aided pattern design, we integrated TFF into the apparel with an embroidery machine, sewing TFF patterns onto the arms, chest, sides, and abdomen (Figure S37a). The TFF embroidery is incorporated into the apparel's outer layer by braiding it on the front and reinforcing it with sewing thread (conductive yarn) on the backside (Figures S37b and S37c). This stitching is robust enough to withstand intense folding and twisting without damage (Figures S37d and S37e). By recording the open-circuit voltage output of the SCA under different magnetic field strengths, we found a clear correlation: the more robust the magnetic field, the higher the output voltage (Figures S37f, S37g, and Video 3).

To further improve the SCA's flexibility and expand its usage scenarios, we integrated a mobile terminal, Bluetooth module and induction coils into the apparel. By connecting the Bluetooth module to the TFF pattern (induction coil), the open-circuit voltage signal generated by the magnetic field can be wirelessly transmitted to a portable electronic device (Figure 6a i). We applied magnetic fields of 3 Gs and 6 Gs near the SCA and successfully received 1 and 1.5 V open-circuit voltage signals via Bluetooth on a cellphone, thus enabling on-the-go sensing of magnetic fields of different intensities (Figure 6b). In addition, the conductive yarn on the back of the TFF embroidery provides the e-textile with near-field communication (NFC) functionality over long distances (>50 cm) as a relay. When the wireless reader is close to the TFF pattern on the arm, a time-varying magnetic field generates induced currents throughout the conductive yarn's relay. This, in turn, creates simultaneous magnetic "hotspots" at both ends of the relay's TFF pattern, allowing for the emulated card at the chest to connect with the reader wirelessly (Figure 6a ii). In practical scenarios, the user places their cell phone, which acts as an emulated card, at the TFF pattern on the chest and simply approaches the gate sensing area with their arm. This setup enables reading the uniform resource locator (URL) information stored in the cellphone's emulated card, allowing the user to pass through the gate without swiping a physical card (Figure 6c and Video 4).

CONCLUSIONS

By effectively improving the wear strength of the sensor via creating a solid−liquid friction interface, we successfully created a triboelectric ferrofluid fiber sensor exhibiting impressive flexibility, high sensitivity, and robust performance. We achieved a hydrophobic surface (with a hydrophobic angle of 145.7°) for the silicone rubber/ferrofluid triboelectric interface through the impregnation method. This treatment efficiently prevents the degradation of electrical output performance caused by the adhesion of ferrofluid to the silicone rubber fiber. The resultant microstructure from the helix extruder enlarges the contact area of the silicone rubber-ferrofluid friction layer after hydrophobic treatment, thereby increasing the surface charge density. Additionally, to circumvent issues associated with the limited flexibility and electromagnetic shielding effectiveness of solid electrode materials like metals, we introduced ionic hydrogel electrodes. This approach resulted in an open-circuit voltage output enhancement of 50% compared to the conventional electrodes. A soft mold method was designed to enable uniform and secure coating of the hydrogel electrode on the silicone rubber fiber surface, leading to a high stretchability of up to 470%. Based on TFF's sensitivity to various environments, we developed a self-powered smart textile for vulnerable groups such as pregnant women and established an environmental early warning and real-time pulse monitoring system, which

https://doi.org/10.1021/acsnano.4c06225
ACS Nano 2024, 18, 33319−33329

can prevent users from being exposed to harmful strong EMFs, thus, minimizing health risks for both maternal and their fetuses. Lastly, we created a e-textile (i.e., SCA) by integrating TFF into clothing and combining it with mobile terminals, Bluetooth modules, and induction coils. This gives users practical and effective magnetic field sensing and communication options for a range of real-world situations.

EXPERIMENTAL METHODS

Materials. Anhydrous ethanol was purchased from Yangyuan Chemical (Changshu) Co., Ltd.

2-Hydroxy-4-(2-hydroxyethoxy)-2-methylpropiophenone, N,N′-methylenebis (acrylamide), and tannic acid were purchased from Aladdin Reagent (Shanghai) Co., Ltd.

Water-based ferrofluid (Saturated magnetization 440 G) was purchased from Ink King (Japan) Co., Ltd.

Acrylamide was purchased from Titan Technology Co., Ltd.

Ethylene glycol was purchased from Macklin Biochemical Technology Co., Ltd.

Sodium chloride was purchased from Hushi Laboratorial Equipment (Shanghai) Co., Ltd.

All materials or chemicals above were directly used as received without any further purification.

Synthesis of Ionic Hydrogel Solution. NaCl with different weights (0.5 g, 1.0 g, 1.5 g, 2.0 g) were first dissolved in a mixture of deionized water (7 mL) and ethylene glycol (3 mL). Then, acrylamide (2.13 g), N,N′-methylenebis (acrylamide) (0.01 g), and tannic acid (0.015 g), and 2-Hydroxy-4-(2-hydroxyethoxy)-2-methyl propiophenone (0.1 g) were added in sequence and stirred until completely dissolved to obtain ionic hydrogel solutions with different concentrations of sodium chloride.

Synthesis of TFF. First, silicone rubber fibers of 2 mm in diameter (thickness of 0.5 mm) with wrinkled inner-wall were oxygen plasma treated and then saturated in a silicon-based super hydrophobic coating solution to soak for a specified duration, and later air-dried. The processed fibers were then immersed in an acidic perfluorodecyltrimethoxysilane ethanol solution, resulting in a hydrophobic coating on the silicone rubber fiber's inner wall. Following this, a water-based ferrofluid was injected into the hollow fiber, which was subsequently sealed using a hot-melt glue to form a friction core layer that boasted a solid−liquid interface. This sealed triboelectric core layer was then treated with plasma and encased in an external hose mold. The gap between the core and the mold was filled with a liquid ionic hydrogel and then subjected to UV light in a curing box to transform the fluid hydrogel into a solid gel state. Finally, the hose mold was peeled off and the Triboelectric Ferrofluid Fiber (TFF).

Morphology Characterization. The surface morphology of the inner wall of silicone rubber fibers before and after hydrophobic treatment was characterized by the desktop scanning electron microscope (Phenom G2 pro).

The contact angles of the inner wall of silicone rubber fibers before and after hydrophobic treatment were tested by the OCA40Micro automatic video microcontact angle measuring instrument.

The cross-sectional morphology of hydrophobic treated silicone rubber fiber and hydrogel coated silicone rubber fiber was characterized by an ultradepth microscope (Leica DVM6) to explore the combination of hydrophobic coating and hydrogel electrode with silicone rubber fiber.

Conductivity Measurement. The electrical conductivity (σ) of hydrogels with different ion concentrations was measured by the Autolab PGSTAT302N electrochemical workstation, and the conductivity was calculated according to the formula:

$$\sigma = L/(S \times R)$$

where L, S, and R are the length, cross-sectional area, and electrical resistance of hydrogels, respectively.

Mechanical Measurement of Hydrogel. The Stretchability of hydrogel samples (thickness of 1 mm) under different aging times and the tensile strength of TFF sample (length of 10 mm) with different tensile rates were measured with the Instron electronic universal testing machine.

Electrical Output Measurement of TFF. The TFF was fixed on one side of the linear motor, and a magnet was fixed on the other side for a controlled reciprocating motion, changing the distance between the TFF and the magnet and recording the speed and distance. The electrical output of TFF was measured by the electrometer (Keithley6514A). When testing and exploring the electrical output performance of frictional electric fibers under different conditions, the speed, displacement, electrical, and optical signals can be transmitted to the computer at the same time and plotted in real time.

ASSOCIATED CONTENT

Supporting Information

The Supporting Information is available free of charge at https://pubs.acs.org/doi/10.1021/acsnano.4c06225.

Stableelectrical output when the phone is inactive (MP4)

Electricaloutput signal is generated by human artifacts through control experiments (MP4)

Open-circuitvoltage output of the SCA under different magnetic field strengths (MP4)

Uniformresource locator (URL) information stored in the cellphone's emulated card (MP4)

Additional data and analyses that complement the main findings of this study; tables comparing response time and sensitivity of various magnetic field sensors, as well as detailed figures on cell viability, structural integrity, resistance measurements, and mechanical stability of hydrogel electrodes; cyclic performance data and open-circuit voltage outputs under various environmental conditions; morphological adaptations of ferrofluid and silicone rubber fibers under stress, as well as the durability and EMI shielding performance of the triboelectric ferrofluid fiber (TFF) system (PDF)

AUTHOR INFORMATION

Corresponding Authors

Yaogang Li − *State Key Laboratory for Modification of Chemical Fibers and Polymer Materials, College of Materials Science and Engineering, Donghua University, Shanghai 201620, China*; Email: yaogang_li@dhu.edu.cn

Wei Gong − *Anhui Provincial Engineering Center for High Performance Biobased Nylons, Anhui Provincial Engineering Center for Automotive Highly Functional Fiber Products, School of Materials and Chemistry, Anhui Agricultural University, Hefei 230036, China; Key Laboratory of Agricultural Sensors, Ministry of Agriculture and Rural Affairs, Hefei 230036, China*; orcid.org/0009-0008-2030-6900; Email: gongw@ahau.edu.cn

Authors

Naiyan Wu − *Anhui Provincial Engineering Center for High Performance Biobased Nylons, Anhui Provincial Engineering Center for Automotive Highly Functional Fiber Products, School of Materials and Chemistry, Anhui Agricultural University, Hefei 230036, China; State Key Laboratory for Modification of Chemical Fibers and Polymer Materials, College of Materials Science and Engineering, Donghua University, Shanghai 201620, China; Department of Electrical and Systems Engineering, Washington University in St. Louis, St. Louis, Missouri 63130-4899, United States*

Pengxiang Mao − *Anhui Provincial Engineering Center for High Performance Biobased Nylons, Anhui Provincial*

https://doi.org/10.1021/acsnano.4c06225
ACS Nano 2024, 18, 33319−33329

Engineering Center for Automotive Highly Functional Fiber Products, School of Materials and Chemistry, Anhui Agricultural University, Hefei 230036, China

Ningbo Chang − *Anhui Provincial Engineering Center for High Performance Biobased Nylons, Anhui Provincial Engineering Center for Automotive Highly Functional Fiber Products, School of Materials and Chemistry, Anhui Agricultural University, Hefei 230036, China*

Yanrun Zhou − *Department of Biomedical Engineering, Washington University in St. Louis, St. Louis, Missouri 63130-4899, United States*

Weifeng Yang − *State Key Laboratory for Modification of Chemical Fibers and Polymer Materials, College of Materials Science and Engineering, Donghua University, Shanghai 201620, China*

Fan Fu − *Anhui Provincial Engineering Center for High Performance Biobased Nylons, Anhui Provincial Engineering Center for Automotive Highly Functional Fiber Products, School of Materials and Chemistry, Anhui Agricultural University, Hefei 230036, China*

Xixi Liu − *Anhui Provincial Engineering Center for High Performance Biobased Nylons, Anhui Provincial Engineering Center for Automotive Highly Functional Fiber Products, School of Materials and Chemistry, Anhui Agricultural University, Hefei 230036, China*

Tianyi Ji − *State Key Laboratory for Modification of Chemical Fibers and Polymer Materials, College of Materials Science and Engineering, Donghua University, Shanghai 201620, China*

Junyi Zhao − *Department of Electrical and Systems Engineering, Washington University in St. Louis, St. Louis, Missouri 63130-4899, United States;* orcid.org/0000-0001-6941-0559

Yuxuan Huang − *Department of Biomedical Engineering, Washington University in St. Louis, St. Louis, Missouri 63130-4899, United States*

Michael D. Dickey − *Department of Chemical and Biomolecular Engineering, North Carolina State University, Raleigh, North Carolina 27695-7905, United States;* orcid.org/0000-0003-1251-1871

Complete contact information is available at: https://pubs.acs.org/10.1021/acsnano.4c06225

Author Contributions

[7]N.W., P.M., and N.C. contributed equally

Notes

The authors declare no competing financial interest.

ACKNOWLEDGMENTS

W.G. acknowledges the financial support by Anhui Provincial Natural Science Foundation (2308085QE147), University Natural Science Research Project of Anhui Province (2023AH051006), National Natural Science Foundation of China (52403260), Textile Vision Basic Research Program (J202410), Opening Fund of China National Textile and Apparel Council Key Laboratory of Flexible Devices for Intelligent Textile and Apparel, Soochow University, No. SDHY2305.

REFERENCES

(1) Sedgh, G.; Singh, S.; Hussain, R. Intended and Unintended Pregnancies Worldwide in 2012 and Recent Trends. *Stud. Fam. Plan.* **2014**, *45* (3), 301−314.

(2) Runkle, J.; Sugg, M.; Boase, D.; Galvin, S. L.; C. Coulson, C. Use of wearable sensors for pregnancy health and environmental monitoring: Descriptive findings from the perspective of patients and providers. *Digit. Health* **2019**, *5*, 14.

(3) Ullah, F.; Iqbal, A.; Iqbal, S.; Kwak, D.; Anwar, H.; Khan, A.; Ullah, R.; Siddique, H.; Kwak, K. S. A Framework for Maternal Physical Activities and Health Monitoring Using Wearable Sensors. *Sensors* **2021**, *21* (15), 4949.

(4) Li, D. K.; Chen, H.; Ferber, J. R.; Odouli, R.; Quesenberry, C. Exposure to Magnetic Field Non-Ionizing Radiation and the Risk of Miscarriage: A Prospective Cohort Study. *Sci. Rep* **2017**, *7*, 7.

(5) Su, X. J.; Yuan, W.; Tan, H.; Liu, X. Y.; Li, D.; Li, D. K.; Huang, G. Y.; Zhang, L. W.; Miao, M. H.; Scarfi, M. R. Correlation between Exposure to Magnetic Fields and Embryonic Development in the First Trimester. *PLoS One* **2014**, *9* (6), No. e101050.

(6) Kashani, Z. A.; Pakzad, R.; Fakari, F. R.; Haghparast, M. S.; Abdi, F.; Kiani, Z.; Talebi, A.; Haghgoo, S. M. Electromagnetic fields exposure on fetal and childhood abnormalities: Systematic review and meta-analysis. *Open Med.* **2023**, *18* (1), 24.

(7) Ryu, D.; Kim, D. H.; Price, J. T.; Lee, J. Y.; Chung, H. U.; Allen, E.; Walter, J. R.; Jeong, H.; Cao, J. Y.; Kulikova, E.; et al. Comprehensive pregnancy monitoring with a network of wireless, soft, and flexible sensors in high- and low-resource health settings. *Proc. Natl. Acad. Sci. U. S. A.* **2021**, *118* (20), 11.

(8) Li, X. Q.; Lu, Y.; Fu, X. H.; Qi, Y. J. Building the Internet of Things platform for smart maternal healthcare services with wearable devices and cloud computing. *Futur. Gener. Comp. Syst.* **2021**, *118*, 282−296.

(9) Li, W. L.; Xiao, Z. L.; Zhao, J. Y.; Aono, K.; Pizzella, S.; Wen, Z. C.; Wang, Y.; Wang, C.; Chakrabartty, S. A Portable and a Scalable Multi-Channel Wireless Recording System for Wearable Electromyometrial Imaging. *IEEE Trans. Biomed. Circuits Syst.* **2023**, *17* (5), 916−927.

(10) Zhang, M.; Cao, M. S.; Shu, J. C.; Cao, W. Q.; Li, L.; Yuan, J. Electromagnetic absorber converting radiation for multifunction. *Mater. Sci. Eng. R-Rep.* **2021**, *145*, No. 100627.

(11) Zhao, J.; Kim, C.; Li, W.; Wen, Z.; Xiao, Z.; Wang, Y.; Chakrabartty, S.; Wang, C. 3D E-textile for Exercise Physiology and Clinical Maternal Health Monitoring. *arXiv preprint arXiv:2407.07954* **2024**.

(12) Wang, R.; Hu, S. X.; Zhu, W.; Huang, Y.; Wang, W. H.; Li, Y.; Yang, Y. C.; Yu, J. J.; Deng, Y. Recent progress in high-resolution tactile sensor array: From sensor fabrication to advanced applications. *Prog. Nat. Sci.* **2023**, *33* (1), 55−66.

(13) Zhang, F.; Jin, T. Q.; Xue, Z. G.; Zhang, Y. H. Recent progress in three-dimensional flexible physical sensors. *Int. J. Smart Nano Mater.* **2022**, *13* (1), 17−41.

(14) Lo, L. W.; Zhao, J. Y.; Wan, H. C. A.; Wang, Y.; Chakrabartty, S.; Wang, C. A. An Inkjet-Printed PEDOT:PSS-Based Stretchable Conductor for Wearable Health Monitoring Device Applications. *ACS Appl. Mater. Interfaces* **2021**, *13* (18), 21693−21702.

(15) Wan, H. C.; Zhao, J. Y.; Lo, L. W.; Cao, Y. Q.; Sepúlveda, N.; Wang, C. Multimodal Artificial Neurological Sensory-Memory System Based on Flexible Carbon Nanotube Synaptic Transistor. *ACS Nano* **2021**, *15* (9), 14587−14597.

(16) Lo, L. W.; Zhao, J. Y.; Wan, H. C.; Wang, Y.; Chakrabartty, S.; Wang, C. A Soft Sponge Sensor for Multimodal Sensing and Distinguishing of Pressure, Strain, and Temperature. *ACS Appl. Mater. Interfaces* **2022**, *14* (7), 9570−9578.

(17) Lo, L. W.; Zhao, J. Y.; Aono, K.; Li, W. L.; Wen, Z. C.; Pizzella, S.; Wang, Y.; Chakrabartty, S.; Wang, C. Stretchable Sponge Electrodes for Long-Term and Motion-Artifact-Tolerant Recording of High-Quality Electrophysiologic Signals. *ACS Nano* **2022**, *16* (8), 11792−11801.

(18) Shen, G. Z. Recent advances of flexible sensors for biomedical applications. *Prog. Nat. Sci.* **2021**, *31* (6), 872−882.
(19) Xu, J.; Tat, T.; Yin, J. Y.; Ngo, D.; Zhao, X.; Wan, X.; Che, Z. Y.; Chen, K. R.; Harris, L.; Chen, J. A textile magnetoelastic patch for self-powered personalized muscle physiotherapy. *Matter* **2023**, *6* (7), 2235−2247.
(20) Zhao, X.; Zhou, Y. H.; Xu, J.; Chen, G. R.; Fang, Y. S.; Tat, T.; Xiao, X.; Song, Y.; Li, S.; Chen, J. Soft fibers with magnetoelasticity for wearable electronics. *Nat. Commun.* **2021**, *12* (1), 11.
(21) Zhou, Y. H.; Zhao, X.; Xu, J.; Fang, Y. S.; Chen, G. R.; Song, Y.; Li, S.; Chen, J. Giant magnetoelastic effect in soft systems for bioelectronics. *Nat. Mater.* **2021**, *20* (12), 1670.
(22) Zhao, J.; Preechayasomboon, P.; Christensen, T.; Memar, A. H.; Shen, Z.; Colonnese, N.; Khbeis, M.; Zhu, M. TouchpadAny-Wear: Textile-Integrated Tactile Sensors for Multimodal High Spatial-Resolution Touch Inputs with Motion Artifacts Tolerance. In *Proceedings of the 37th Annual ACM Symposium on User Interface Software and Technology*; ACM Digital Library 2024.
(23) Zhang, S. Y.; Chen, Y. J.; Wang, D. Y.; He, P. Solid-liquid contact TENG using a melting near-field direct writing PCL nanofiber structure. *Int. J. Smart Nano Mater.* **2023**, *14* (1), 90−102.
(24) Gong, W.; Hou, C.; Zhou, J.; Guo, Y.; Zhang, W.; Li, Y.; Zhang, Q.; Wang, H. Continuous and scalable manufacture of amphibious energy yarns and textiles. *Nat. Commun.* **2019**, *10* (1), 868.
(25) Gong, W.; Wang, X.; Yang, W.; Zhou, J.; Han, X.; Dickey, M. D.; Su, Y.; Hou, C.; Li, Y.; Zhang, Q.; Wang, H. Wicking-Polarization-Induced Water Cluster Size Effect on Triboelectric Evaporation Textiles. *Adv. Mater.* **2021**, *33* (15), No. e2007352.
(26) Dong, K.; Peng, X.; An, J.; Wang, A. C.; Luo, J.; Sun, B.; Wang, J.; Wang, Z. L. Shape adaptable and highly resilient 3D braided triboelectric nanogenerators as e-textiles for power and sensing. *Nat. Commun.* **2020**, *11* (1), 2868.
(27) Liu, J. Y.; Wen, Z.; Lei, H.; Gao, Z. Q.; Sun, X. H. A Liquid-Solid Interface-Based Triboelectric Tactile Sensor with Ultrahigh Sensitivity of 21.48 kPa^{-1}. *Nano-Micro Lett.* **2022**, *14* (1), 11.
(28) Chang, J.; Zhai, H.; Hu, Z.; Li, J. Ultra-thin metal composites for electromagnetic interference shielding. *Compos. Pt. B-Eng.* **2022**, *246*, No. 110269.
(29) Cheng, J. Y.; Li, C. B.; Xiong, Y. F.; Zhang, H. B.; Raza, H.; Ullah, S.; Wu, J. Y.; Zheng, G. P.; Cao, Q.; Zhang, D. Q.; et al. Recent Advances in Design Strategies and Multifunctionality of Flexible Electromagnetic Interference Shielding Materials. *Nano-Micro Lett.* **2022**, *14* (1), 31.
(30) Zhao, Y.; Hao, L. L.; Zhang, X. D.; Tan, S. J.; Li, H. H.; Zheng, J.; Ji, G. B. A Novel Strategy in Electromagnetic Wave Absorbing and Shielding Materials Design: Multi-Responsive Field Effect. *Small Sci.* **2022**, *2* (2), 23.
(31) Chung, D. D. L. Electromagnetic interference shielding effectiveness of carbon materials. *Carbon* **2001**, *39* (2), 279−285.
(32) Dharmasena, R.; Deane, J. H. B.; Silva, S. R. P. Nature of Power Generation and Output Optimization Criteria for Triboelectric Nanogenerators. *Adv. Energy Mater.* **2018**, *8* (31), 11.
(33) Wang, Z. L. Triboelectric nanogenerators as new energy technology and self-powered sensors - Principles, problems and perspectives. *Faraday Discuss.* **2014**, *176*, 447−458.
(34) Trung, T. Q.; Lee, N. E. Flexible and Stretchable Physical Sensor Integrated Platforms for Wearable Human-Activity Monitoring and Personal Healthcare. *Adv. Mater.* **2016**, *28* (22), 4338−4372.
(35) Amjadi, M.; Pichitpajongkit, A.; Lee, S.; Ryu, S.; Park, I. Highly Stretchable and Sensitive Strain Sensor Based on Silver Nanowire-Elastomer Nanocomposite. *ACS Nano* **2014**, *8* (5), 5154−5163.
(36) Sun, C.; Luo, J.; Jia, T.; Hou, C.; Li, Y.; Zhang, Q.; Wang, H. Water-resistant and underwater adhesive ion-conducting gel for motion-robust bioelectric monitoring. *Chem. Eng. J.* **2022**, *431*, No. 134012.
(37) Zhao, J. Y.; Lo, L. W.; Wan, H. C.; Mao, P. S.; Yu, Z. B.; Wang, C. High-Speed Fabrication of All-Inkjet-Printed Organometallic Halide Perovskite Light-Emitting Diodes on Elastic Substrates. *Adv. Mater.* **2021**, *33* (48), 11.
(38) Zhao, J. Y.; Lo, L. W.; Yu, Z. B.; Wang, C. Handwriting of perovskite optoelectronic devices on diverse substrates. *Nat. Photonics* **2023**, *17* (11), 964.
(39) Sanchis, M. R.; Blanes, V.; Blanes, M.; Garcia, D.; Balart, R. Surface modification of low density polyethylene (LDPE) film by low pressure O_2 plasma treatment. *Eur. Polym. J.* **2006**, *42* (7), 1558−1568.
(40) Yin, J.; Lu, C.; Li, C.; Yu, Z.; Shen, C.; Yang, Y.; Jiang, X.; Zhang, Y. A UV-filtering, environmentally stable, healable and recyclable ionic hydrogel towards multifunctional flexible strain sensor. *Compos. Pt. B-Eng.* **2022**, *230*, No. 109528.
(41) Li, T. T.; Hu, X. M.; Zhang, Q. S.; Zhao, Y. Y.; Wang, P.; Wang, X.; Qin, B. T.; Lu, W. Poly(acrylic acid)-chitosan @ tannic acid double-network self-healing hydrogel based on ionic coordination. *Polym. Adv. Technol.* **2020**, *31* (7), 1648−1660.
(42) Calvet, D.; Wong, J. Y.; Giasson, S. Rheological monitoring of polyacrylamide gelation: Importance of cross-link density and temperature. *Macromolecules* **2004**, *37* (20), 7762−7771.
(43) Naghash, H. J.; Okay, O. Formation and structure of polyacrylamide gels. *J. Appl. Polym. Sci.* **1996**, *60* (7), 971−979.
(44) Pragya, A.; Mutalik, S.; Younas, M. W.; Pang, S. K.; So, P. K.; Wang, F. M.; Zheng, Z. J.; Noor, N. Dynamic cross-linking of an alginate-acrylamide tough hydrogel system: time-resolved in situ mapping of gel self-assembly. *RSC Adv.* **2021**, *11* (18), 10710−10726.
(45) Lin, F.; Quraishy, A. N.; Li, R. J.; Yang, G.; Mohebinia, M.; Tong, T.; Qiu, Y.; Vishal, T.; Zhao, J. Y.; Zhang, W.; et al. Molding, patterning and driving liquids with light. *Mater. Today* **2021**, *51*, 48−55.
(46) Lin, F.; Quraishy, A. N.; Tong, T.; Li, R.; Yang, G.; Mohebinia, M.; Qiu, Y.; Vishal, T.; Zhao, J.; Zhang, W.; Zhong, H.; Zhang, H.; Chen, Z.; Zhou, C.; Tong, X.; Yu, P.; Hu, J.; Dong, S.; Liu, D.; Wang, Z.; Schaibley, J. R.; Bao, J.; et al. Marangoni convection-driven laser fountains on free surfaces of liquids. *Materials Today Physics* **2021**, *21*, No. 100558.
(47) Genc, S.; Derin, B. Synthesis and rheology of ferrofluids: a review. *Curr. Opin. Chem. Eng.* **2014**, *3*, 118−124.
(48) Chiolerio, A.; Quadrelli, M. B. Smart Fluid Systems: The Advent of Autonomous Liquid Robotics. *Adv. Sci.* **2017**, *4* (7), 18.
(49) Odenbach, S.; Liu, M. Invalidation of the Kelvin force in ferrofluids. *Phys. Rev. Lett.* **2001**, *86* (2), 328−331.
(50) Petit, M.; Kedous-Lebouc, A.; Avenas, Y.; Tawk, M.; Artega, E. Calculation and analysis of local magnetic forces in ferrofluids. *Prz. Elektrotechniczny* **2011**, *87* (9B), 115−119.
(51) Wenzel, R. N. Resistance of solid surfaces to wetting by water. *Ind. Eng. Chem.* **1936**, *28*, 988−994.
(52) Carlson, S.; Becker, M.; Brünig, F. N.; Ataka, K.; Cruz, R.; Yu, L. X.; Tang, P.; Kanduc, M.; Haag, R.; Heberle, J.; et al. Hydrophobicity of Self-Assembled Monolayers of Alkanes: Fluorination, Density, Roughness, and Lennard-Jones Cutoffs. *Langmuir* **2021**, *37* (47), 13846−13858.
(53) Bourantas, C. V.; Tenekecioglu, E.; Radu, M.; Räber, L.; Serruys, P. W. State of the art: role of intravascular imaging in the evolution of percutaneous coronary intervention - a 30-year review. *EuroIntervention* **2017**, *13* (6), 644−653.
(54) Kivrak, E. G.; Yurt, K. K.; Kaplan, A. A.; Alkan, I.; Altun, G. Effects of electromagnetic fields exposure on the antioxidant defense system. *J. Microsc Ultrastruct* **2017**, *5* (4), 167−176.
(55) Davis, P. L.; Crooks, L.; Arakawa, M.; McRee, R.; Kaufman, L.; Margulis, A. R. POTENTIAL HAZARDS IN NMR IMAGING - HEATING EFFECTS OF CHANGING MAGNETIC-FIELDS AND RF FIELDS ON SMALL METALLIC IMPLANTS. *Am. J. Roentgenol.* **1981**, *137* (4), 857−860.
(56) Fragopoulou, A. F.; Koussoulakos, S. L.; Margaritis, L. H. Cranial and postcranial skeletal variations induced in mouse embryos by mobile phone radiation. *Pathophysiology* **2010**, *17* (3), 169−177.
(57) Schenck, J. F. Safety of strong, static magnetic fields. *J. Magn. Reson. Imaging* **2000**, *12* (1), 2−19.
(58) Driessen, S.; Bodewein, L.; Dechent, D.; Graefrath, D.; Schmiedchen, K.; Stunder, D.; Kraus, T.; Petri, A. K.; Scarfi, M. R.

Biological and health-related effects of weak static magnetic fields (≤ 1 mT) in humans and vertebrates: A systematic review. *PLoS One* **2020**, *15* (6), No. e0230038.
(59) Nam, H.; Seol, K. H.; Lee, J.; Cho, H.; Jung, S. W. Review of Capacitive Touchscreen Technologies: Overview, Research Trends, and Machine Learning Approaches. *Sensors* **2021**, *21* (14), 4776.
(60) Ziegelberger, G.; Vecchia, P.; Hietanen, M.; Ahlbom, A.; Anderson, L. E.; Breitbart, E.; De Gruijl, F. R.; Lin, J. C.; Matthes, R.; Peralta, A. P.; Söderberg, P. GUIDELINES ON LIMITS OF EXPOSURE TO STATIC MAGNETIC FIELDS. *Health Phys.* **2009**, *96* (4), 504−514.

https://doi.org/10.1021/acsnano.4c06225
ACS Nano 2024, 18, 33319−33329